Available online at www.sciencedirect.com
SCIENCE DIRECT®
International Journal of Heat and Mass Transfer 47 (2004) 865–875
International Journal of HEAT and MASS TRANSFER
www.elsevier.com/locate/ijhmt

Heat and mass transfer in vacuum membrane distillation

J.I. Mengual, M. Khayet *, M.P. Godino

Department of Applied Physics I, Faculty of Physics, University Complutense of Madrid, Av. Complutense s/n, Madrid 28040, Spain

Received 1 August 2002; received in revised form 17 September 2002

Abstract

In the membrane distillation (MD) literature, the heat transfer coefficients of the boundary layers are usually estimated from well known heat transfer empirical correlations developed for non-porous and rigid heat exchangers. A difference between the mechanism of heat transfer in MD systems, which is coupled with transmembrane mass transfer, and the mechanism of heat transfer in "pure" heat exchangers is expected to exist. Vacuum membrane distillation has been experimentally studied in a capillary membrane module and the heat transfer coefficients have been evaluated in both the lumen and the shell side of the membrane module. A critical review of the most frequently used heat transfer empirical correlations in MD systems is presented. Finally, the experimental results obtained in this paper are compared to those of literature, in order to test their applicability in membrane distillation systems.

Keywords: Vacuum membrane distillation; Heat and mass transfer

1. Introduction

The separation process known as membrane distillation (MD) usually refers to a thermally driven transport of water vapour through a porous hydrophobic partition [1]. One side of the partition (the feed side) is always in contact with an aqueous solution. The other side (the permeate side) may be brought into contact with four different phases: (1) With an aqueous solution, giving rise to the configuration called direct contact membrane distillation (DCMD). (2) With a sweeping gas. In this case the process is termed Sweeping gas membrane distillation (SGMD). (3) With a stagnant air gap plus a cold plate. This configuration is called air gap membrane distillation (AGMD). (4) With a vacuum volume. The process is called in this case vacuum membrane distillation (VMD). In the first case (DCMD), the transport mechanism is as follows: the membrane material is water repellent, so liquid water cannot enter the pores unless a hydrostatic pressure, exceeding the so-called "liquid entry pressure of water (LEP_w)" is applied [2]. In the absence of such a pressure, a liquid–vapour interface is formed at the entrances of the pores. If a temperature difference is maintained between both sides of the membrane, a water vapour pressure difference appears. As a result, water molecules evaporate at the hot interface, cross the membrane in vapour phase and condense in the cold side. In the other cases, the cold liquid is substituted and the water molecules are removed and recovered in an external condenser. In all cases, there is a net transmembrane water flux.

The process of MD, which may be used to produce ultra-pure water or to get the concentration of a determined non-volatile component from an aqueous solution, may be carried out with the above cited experimental configurations. Each one of these possibilities has its advantages and inconveniences [1]. In a VMD configuration, the diffusion of the water vapour inside the pores is favoured. In addition, there is not boundary layer in the vacuum side and this implies a decrease in the heat conducted through the membrane. In other words, this configuration combines two advantages: a very low conductive heat loss with a reduced mass transfer resistance. But there is one inconvenience:

* Corresponding author. Tel.: +34-91-3944454; fax: +34-91-3945191.
E-mail address: khayetm@fis.ucm.es (M. Khayet).

0017-9310/$ - see front matter © 2003 Elsevier Ltd. All rights reserved.
doi:10.1016/j.ijheatmasstransfer.2002.09.001

Nomenclature

a	characteristic constant
B	global MD coefficient (kg/m^2 s Pa)
B'	net MD coefficient (kg/m^2 s Pa)
b	characteristic constant
c	characteristic constant
d_h	hydraulic diameter (m)
Gr	Grashof number
Gz	Graetz number
h_w	heat transfer coefficient (W/m^2 K)
ΔH_v	heat of vapourisation of water (J/kg)
j	number of experimental data points
k_w	thermal conductivity of water (W/m K)
L	channel length (m)
M	molecular mass of water (kg/mol)
N	MD water flux (kg/m^2 s)
Nu	Nusselt number
P	pressure (Pa)
Pr	Prandtl number
P_v	water vapour pressure (Pa)
P_0	vacuum pressure (Pa)
r	pore size (m)
R	gas constant (J/mol K)
Re	Reynolds number
T	temperature (K)
T_w	temperature of the water in the bulk phase (K)
T'_w	temperature of the water in the membrane surface (K)
v_w	water circulation velocity (m/s)

Greek symbols

δ	membrane thickness (m)
ε	fractional void volume
λ	mean free path of water molecule (m)
μ_w	water dynamic viscosity (kg/m·s)
θ	yaw angle of the membrane module
σ_w	minimum weighted standard deviation
τ	pore tortuosity

the existence of a vacuum side may favour the wetting of the membrane pores. An examination of the literature permits to assert that the DCMD has been the configuration more studied, as opposed with the VMD, which has deserved less attention.

On the other hand, in the MD literature, the heat transfer coefficients of the boundary layers are usually estimated from well-known heat transfer empirical correlations. These correlations have been obtained, and, consequently, are valid only for non-porous and rigid heat exchangers. On the contrary, the membrane surface is porous and not rigid. So, in principle, it is expected to exist a difference between the mechanisms of heat transfer in MD systems and in "pure" heat exchangers, for which the correlation equations were developed. In addition, in a MD system, the heat transfer is coupled with a mass transfer [1]. As a consequence, the applicability of those empirical correlations to MD processes should be questioned.

With this in mind, in the present paper we have studied the VMD phenomenon in a shell-and-tube capillary membrane module and using pure water as feed solution. This module resembles the shell-and-tube heat exchangers, except that capillary membranes replace the impermeable tubes. Different experimental conditions referring to temperature and water circulation velocity inside the module, both in the lumen and in the shell side have been considered. A procedure, which permits to calculate the liquid heat transfer coefficient in both shell and lumen side of the membrane module, has been used. The temperature polarisation effect, the mechanisms of heat and mass transfer through the system and the physical nature of the transmembrane flow have been considered. The experimental heat transfer equations, obtained in terms of Nusselt, Reynolds and Prandtl numbers, were compared with the heat transfer empirical correlations most frequently used in MD publications.

2. Experimental

The experimental device used may be seen in Fig. 1. The central part is a commercial shell-and-tube capillary membrane module MD020CP2N, supplied by Mycrodyn. Basically it consists of a set of equal polypropylene porous hydrophobic capillaries. Its principal characteristics, as specified by the manufacturer, are as follows:

Number of capillaries: 40; membrane pore size: 0.2 μm; inner capillary diameter: 1.8 mm; outer capillary diameter: 2.6 mm; effective filtration area of the membrane: 0.1 m^2; LEP_w: 140 kPa; fractional void volume: 70%; length of capillaries: 470 mm.

Pure water (deionised and distilled) was employed in the experiments.

The temperature of the liquid feed was measured at the inlet and at the outlet of the membrane module. These temperatures were measured continuously, in steady state, with Pt100 probes connected to a digital multimeter Keithley 199, with an accuracy of ±0.1 °C. The liquid inlet temperature was controlled by a thermostat Lauda K20KS connected to a heat exchanger located between the pump and the membrane module.

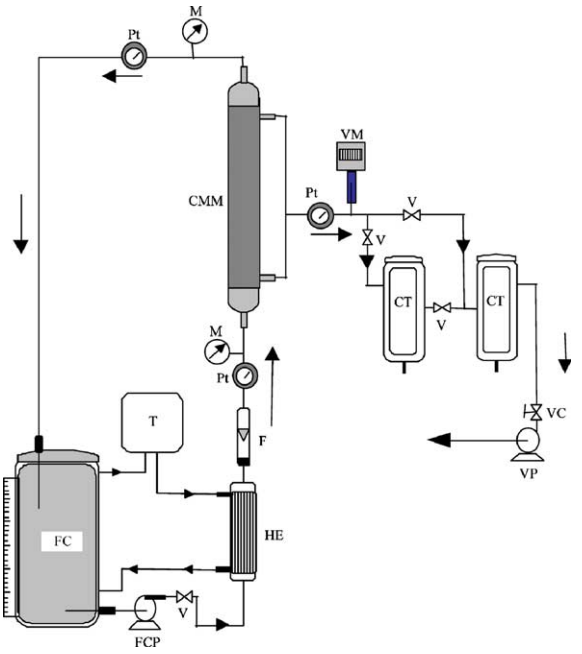

Fig. 1. Schema of the experimental set-up. (CMM) capillary membrane module; (FC) feed container; (HE) heat exchanger; (T) thermostat; (FCP) feed circulation pump; (V) valve; (F) flowmeter; (CT) cold trap; (VP) vacuum pump; (VM) vacuum manometer; (VC) vacuum controller; (M) manometer and (Pt) Pt-100 probe.

The liquid feed was circulated with a circulation pump March TE-5.5C.MD and the feed flow was measured with a flowmeter Tecfluid TCP 316-0630, with precision ±2%. The volume of water in the feed side was measured with a graduate tube connected to the feed container. The whole system was entirely insulated in order to minimise the heat lost to the surroundings.

A vacuum pump (MacLeod Model B2) with a pressure controller was connected to the permeate side of the membrane module to remove the water vapour flux. Two glass cold traps containing liquid nitrogen were connected in series to recover the water vapour. A calibrated vacuum manometer Wika Tronic Transmitter was used to measure the pressure at the permeate side of the module. The pressure gradient through the membrane was controlled continuously with two manometers placed in the feed side, at the inlet and outlet of the module.

The flux of distilled water was calculated, in every case, by measuring the decrease of the feed volume every ten minutes, during three hours, and adjusting the experimental pairs of data {volume-time} to a straight line by a least squares method. The correlation coefficient was always better than 0.999, which means that the procedure is adequate. The total volume of water lost in the feed container was compared to the volume of permeate collected and weighted at the end of each experimental run. The agreement was good (5% in the worst case). In fact, these procedures permit to detect any membrane wetting as well as any water lost evaporated from the feed container. Note that in Fig. 1, the feed liquid is circulated in the lumen side and vacuum is applied in the shell side of the membrane module. Changing the connections of the tubes permits to get the configuration corresponding to water flowing in shell side.

3. Theory

The system to be studied consists of an array of capillary porous hydrophobic membranes, assembled together in a shell-and-tube module. Each membrane is held between two chambers. One of the chambers is circulated by hot water and the other is connected to a vacuum pump. In these conditions, a transmembrane water vapour pressure difference is created. Mass transfer through the membrane, by a MD mechanism, takes place due to the convective and/or diffusive transport of water vapour across the membrane pores, the driving force being the difference in vapour pressure.

The transmembrane mass transfer, in a general MD process, may be explained, in principle, according to different possibilities [1,3–5]: the Knudsen flow model, the Poiseuille flow model, the diffusion-in-air flow model, or any combination among them. In a VMD configuration, the molecular diffusion model is not adequate due to the very low value of the partial pressure of the air inside the pores. Consequently, the Knudsen and Poiseuille models should be chosen as more appropriated. These models suggest a linear relationship between the water flux, N, and the transmembrane water vapour pressure difference, $\Delta P'$ [1–3]:

$$N = B'\Delta P' = B'[P_v(T'_w) - P_0] \tag{1}$$

where B' is called net MD coefficient, P_0 is the pressure in the vacuum side and $P_v(T'_w)$ is the water vapour pressure in the membrane surface, at the temperature T'_w. Coefficient B' depends on temperature as well as on some geometric characteristics of the membrane.

As it is well known, the water vapour pressure at the liquid/vapour interface (in Pa) may be related with the temperature (in K), by using the Antoine's equation:

$$P_v(T) = \exp\left(23.1964 - \frac{3816.44}{-46.13 + T}\right) \tag{2}$$

When writing Eq. (2), the curvature of the liquid/vapour surface is assumed to have negligible effects on the equation as compared to the flat surface state [1].

In the present VMD configuration, with a membrane having small pores, the mean free path of water molecules, λ, can reach relatively high values, because of the dependence of λ on P^{-1}. In the considered conditions, for temperatures ranging between 30 and 65 °C, the mean free path of water molecules varies between 2.8 and 3.4 μm. On the other hand, the pore size of the membrane is 0.2 μm. This means that the Knudsen number, defined as the ratio between the mean free path and the pore size, varies from 14 to 17. Consequently, the molecule-pore wall collisions are dominant with respect to the molecule-molecule collisions. In this case, the Kinetic Theory of Gases, or more exactly the Dusty Gas Model, suggest that there is a Knudsen type diffusion of water molecules through the membrane pores and the following explicit expression for the coefficient B' is achieved [1,3,6,7]:

$$B' = 1.064 \cdot \frac{r\varepsilon}{\delta\tau} \cdot \left(\frac{M}{RT}\right)^{1/2} \tag{3}$$

In this equation, r is the pore size, ε is the fractional void volume of the membrane, δ is the membrane thickness, τ is the pore tortuosity, M is the water molecular mass and R is the gas constant.

It is worth quoting that in a VMD process, there is a heat transfer coupled with the mass transfer. This heat transfer occurs by two major mechanisms [1,3]: (1) the latent heat transfer accompanying the transmembrane vapour flux, and (2) the heat transferred by conduction through the membrane matrix. Consequently, there is a rather complex relationship between both heat and mass transfer. This problem is related and involved with the presence of an unstirred boundary layer that adjoins the membrane at the feed side. This implies that the temperature at the membrane surface, T'_w, is lower than the corresponding value at the well-stirred bulk phase, T_w. The phenomenon is called "temperature polarisation" and masks the real magnitude of the driving force [1–3,8–10].

The transmembrane flux may be related with h_w, the heat transfer coefficient of the water in the layer, from the feed bulk to the membrane surface. In order to do that, we must equalise, in steady state, the heat transferred through the liquid boundary layer and the energy transported through the membrane [3,11]:

$$h_w(T_w - T'_w) = N\Delta H_v \tag{4}$$

where ΔH_v is the heat of vapourisation of water. In the last equation, the contribution of the heat conducted through the membrane matrix has been neglected, according to [1,11]. It is worth noticing that the value of T_w can be measured but, on the contrary, T'_w cannot be, due to the presence of the feed boundary layer.

The numerical influence of the temperature polarisation effect may be taken into account by two methods:

(1) By means of an iterative method from Eqs. (1)–(3). In order to do that, a temperature corresponding to the mean value between the temperatures in both chambers was used as a first choice. This value was used in Eq. (3) to obtain a first value of the coefficient B'. Then, according to Eq. (1), the obtained value of B' was used to get a value of $P_v(T'_w)$. Finally, Antoine's equation (2) is used to get a new value of T'_w. This process is repeated many times until an invariant value of the temperature, at the membrane surface, is reached. Then, the heat transfer coefficient may be calculated according to Eq. (4) and converted into the corresponding value of the Nusselt number, $Nu = h_w \cdot d_h/k_w$, being d_h the hydraulic diameter and k_w the thermal conductivity.

(2) Eq. (1) may be rewritten as [1–5]:

$$N = B'\Delta P' = B\Delta P \tag{5}$$

where B' is the net MD coefficient, B is the global MD coefficient, which takes into consideration the temperature polarisation and can be easily calculated from the experimental data; $\Delta P'$ is the transmembrane vapour pressure difference between the membrane surface and the permeate side and ΔP is the vapour pressure difference between the bulk phase and the permeate side.

As it is well known, the MD experiments state that the MD flux and, consequently, the global MD coefficient increase with the water circulation velocity. This is due to the decrease of the temperature polarisation effects. The contribution of the boundary layers to the decrease of the thermal effects in MD has been studied extensively [1–5,7–13]. The method proposed is based on the fact that the thickness of the boundary layer decreases with the flow rate (i.e. circulation velocity). By performing measurements of the MD flux at different circulation velocities and extrapolating the data to an infinite velocity, the temperature polarisation effect was estimated.

In previous papers [2,12] the following relationship can be achieved.

$$\frac{1}{N} = A_0 + \frac{A_1}{v_w^n} \tag{6}$$

where A_0 and A_1 are functions depending on the system parameters, v_w is the circulation velocity and n is a positive dimensionless number. Eq. (6) was obtained from the study of heat transfer through the thermal boundary layer and from the dependence of the Nusselt number, which is proportional to the heat transfer coefficient, on the Reynolds number, which is proportional to the circulation velocity. According to Eq. (6), the value of the MD flux that would correspond to an infinite circulation velocity (N_∞), in absence of polarisa-

tion effects, may be obtained from the parameter A_0 ($A_0 = 1/N_\infty$). In this case the temperature polarisation coefficient is the ratio N_0/N_∞.

For a given transmembrane vapour pressure, Eq. (6) may be written as

$$\frac{1}{B} = A'_0 + \frac{A'_1}{v_w^n} \tag{7}$$

where A'_0 and A'_1 are functions depending on the system parameters. From the value A'_0, the net MD coefficient, B', may be obtained ($B' = 1/A'_0$).

As it has been already said, the heat transfer coefficients are usually estimated, in MD studies, from the "adequate" empirical correlations according to the flow regime. These correlations were obtained for non-porous and rigid heat exchangers. On the contrary, the membrane surface is porous and not rigid, so, in principle, those correlations could not be valid as the experimental conditions are different.

The empirical equations employed are usually written in this simplified form:

$$Nu = a \cdot Re^b \cdot Pr^c \tag{8}$$

where, Re and Pr are the Reynolds and Prandtl numbers, and a, b, and c are characteristic constants of the module design and liquid flow regime [14,15].

In what follows, the most useful correlation equations employed in MD studies will be listed. It is worth quoting that the liquid feed may be circulated along the shell side or in the lumen side. This can influence the heat transfer mechanism. Consequently, both possibilities will be considered separately:

3.1. Internal flow (liquid flowing in the lumen side)

3.1.1. Laminar flow

In this case the Nusselt number increases with the quantity ($Re \cdot Pr \cdot d_h/L$), where L is the channel length. At high values of this quantity, the Hausen equation was used in Refs. [10,16]:

$$Nu = 3.66 + \frac{0.0668 \cdot (Re \cdot Pr \cdot d_h/L)}{1 + 0.045 \cdot (Re \cdot Pr \cdot d_h/L)^{2/3}} \tag{9}$$

Other authors [17,18] utilise the equation:

$$Nu = 4.36 + \frac{0.036 \cdot (Re \cdot Pr \cdot d_h/L)}{1 + 0.0011 \cdot (Re \cdot Pr \cdot d_h/L)^{0.8}} \tag{10}$$

It is worth noticing that the Nusselt number approaches asymptotically to a lower limiting value as the quantity ($RePrd_hL$) is reduced. This value is 4.36 for constant heat flux and is 3.66 for constant surface temperature [14].

For low values of the quantity ($RePrd_hL$), the Sieder and Tate equation was used in Refs. [19,20]:

$$Nu = 1.86 \cdot (Re \cdot Pr \cdot d_h/L)^{1/3} \tag{11}$$

The Léveque equation has been also utilised in Refs. [21–23]:

$$Nu = 1.62 \cdot (Re \cdot Pr \cdot d_h/L)^{1/3} \tag{12}$$

If the influence of the free convection is important, the following relationship was proposed in Refs. [17,24]:

$$Nu = 1.75 \cdot \{Gz + 0.04 \cdot [(d_h/L) \cdot Gr \cdot Pr]^{0.75}\}^{1/3} \tag{13}$$

where Gz is the Graetz number, and Gr is the Grashof number [14,15].

In all these equations, the bulk temperature is used. If a great temperature difference between the bulk and the membrane wall is present, most authors employ a correction factor $(\mu_w/\mu'_w)^{0.14}$ in the right side of the equations, where μ_w is the water dynamic viscosity at the bulk phase and μ'_w is the corresponding value at the membrane surface.

3.1.2. Turbulent flow

The phenomena involved in the case of turbulent forced convection are very complexes and different empirical equations have been used. For example, the Dittus–Boelter equation was utilised in Refs. [1,3,19]:

$$Nu = 0.023 \cdot Re^{4/5} \cdot Pr^m \tag{14}$$

where m is 0.4, for heating, and 0.3, for cooling.

A different possibility, the correlation proposed by Sieder and Tate [14], was proposed to perform MD theoretical models in Ref. [1]:

$$Nu = 0.027 \cdot Re^{4/5} \cdot Pr^{1/3} (\mu_w/\mu'_w)^{0.14} \tag{15}$$

The above equations may be modified to take into account the entrance effects, which are important in the case of short tubes [1,14,15].

3.1.3. Transitional flow

In this case, the heat transfer coefficients are difficult to predict because of the fluctuations in the heat transfer and the instabilities in the flow. One attempt of correlation for this region is due to Hausen [25]:

$$Nu = 0.116 \cdot (Re^{2/3} - 125) \cdot Pr^{1/3} \cdot [1 + (d_h/L)^{2/3}] \cdot (\mu_w/\mu'_w)^{0.14} \tag{16}$$

It is worth quoting that this equation has received no attention, in studies of MD, in spite of the fact that most of MD systems have Reynolds numbers in this range.

3.2. External flow (liquid flowing in the shell side)

As it has been already said, in the case of MD tubular modules, the heat transfer mechanism is different when the liquid flows in the shell side or in the tube side.

For flows in the shell side of capillaries tubular modules, parallel and cross flow may occur simultaneously. In these cases, Groehn proposed the following correlation for cylindrical heat exchangers that are not normal to the flow:

$$Nu = 0.206 \cdot (Re \cdot \cos\theta)^{0.63} \cdot Pr^{0.36} \quad (17)$$

where θ is the yaw angle, which varies between 0°, for pure cross-flow, and 90°, for pure parallel flow [14].

4. Results and discussion

In the present paper, the MD flux has been measured for different values of the circulation velocity and the temperature of the feed at the inlet of the membrane module. The influence of the vacuum pressure in the permeate side was extensively studied by other authors in previous works [7,26]. It is worth quoting that the hydraulic circulation conditions vary depending whether the feed is circulated in the shell side or in the lumen side of the membrane module. According to this, two sets of experiments were carried out. Each set consists of two series of experiments. In the first series, the feed circulation velocity was varied between 0.2 and 1.0 m/s for each one of the following water inlet temperatures: 40, 50, 60 and 65 °C. In this case, the generated Reynolds numbers range from 570 to 4831, for water flowing in the lumen side and from 268 to 2263, for water flowing in the shell side. In the second series, the water inlet temperature was varied between 35 and 65 °C, with steps of 5 K, for feed circulation velocities 0.6 and 1.0 m/s, to give Prandtl numbers ranging between 5 and 2.7. In all the experiments, the pressure in the vacuum side was maintained constant to a value of 4000 Pa with precision ±5%.

The purposes of these sets of measurements were: (i) to study the influence of the varying parameters, water tangential velocity and temperature, on the MD flux; (ii) to calculate the heat transfer coefficient of the boundary layer, as function of these parameters, and (iii) to test the applicability of the empirical correlations presented in the Section 3 to VMD processes.

The experimental results may be seen in Figs. 2–4. It must be pointed out that the error bars corresponding to each point have not been shown because they are approximately equal to the size of the points (<4%).

Figs. 2 and 3 show the experimental values of the MD flux as function of the water circulation velocity, with the liquid inlet temperature as parameter. Fig. 2 refers to the water circulating in the shell side and Fig. 3 in the lumen side. In both cases the MD flux increases with the feed circulation velocity and with the water inlet temperature. This trend has been reported previously for various MD processes in Refs. [1,2,7,11,27]. The dependence of the MD flux on the circulation velocity confirms the presence of the boundary layers in the feed

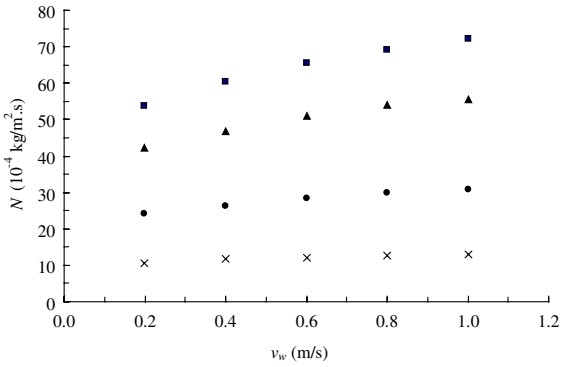

Fig. 2. MD flux (N) as function of the water circulation velocity (v_w) through the shell side of the membrane module, for different water inlet temperatures (T_{win}): (×) for $T_{win} = 40$ °C; (●) for $T_{win} = 50$ °C; (▲) for $T_{win} = 60$ °C and (■) for $T_{win} = 65$ °C.

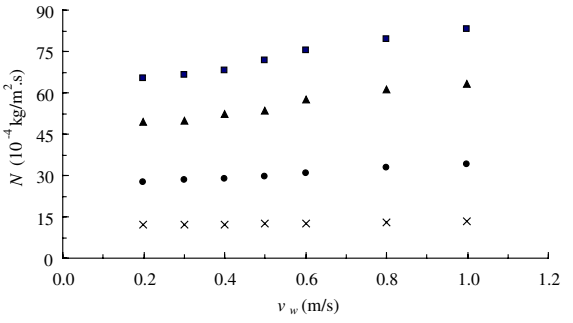

Fig. 3. MD flux (N) as function of the water circulation velocity (v_w) through the lumen side of the membrane module, for different water inlet temperatures (T_{win}): (×) for $T_{win} = 40$ °C; (●) for $T_{win} = 50$ °C; (▲) for $T_{win} = 60$ °C and (■) for $T_{win} = 65$ °C.

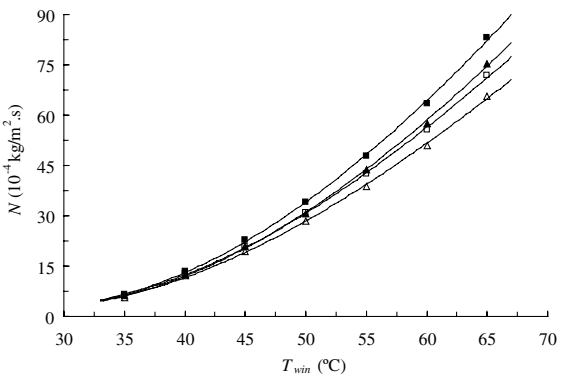

Fig. 4. MD flux (N) as function of the water inlet temperature (T_{win}), for water circulation velocity (v_w) of 0.6 m/s (△, ▲) and 1 m/s (□, ■). (△, □) for water in shell side and (▲, ■) for water in lumen side. The lines are the Arrhenius fits of the data.

side. Besides, the relative influence of the feed circulation velocity on the MD flux increases with the temperature. This effect can be attributed to the higher water vapour pressure sensitivity at higher temperatures. Moreover, the MD flux is greater when the liquid feed is circulated in the lumen side than in the shell side. This may be due to the higher Reynolds numbers achieved when water is circulating in the lumen side of the membrane module in comparison to the shell side Reynolds numbers. At higher Reynolds numbers higher heat transfers from the bulk feed to the membrane surface and the temperature at the membrane surface approaches to the corresponding temperature in the bulk phases leading to greater MD flux. It must be mentioned that the temperature drop observed at the feed side between the inlet and the outlet of the membrane module is lower in the case of water flowing in the lumen side than in the shell side: 2.7–5.8% (lumen side) as compared with 4.1–7.5% (shell side). These numerical values are dependent on the water inlet temperature and circulation velocity.

Fig. 4 shows the experimental values of the MD flux as function of the water inlet temperature, with the feed circulation velocity as a parameter, for either shell and lumen flow sides of the membrane module. Again, the data show that the MD flux increases with both the feed circulation velocity and the water inlet temperature. This behaviour, which has been observed in DCMD [19] and SGMD [4,5] configurations, may be explained by the exponential relationship between temperature and vapour pressure shown in Eq. (2). The lines in Fig. 4 represent the fit of the experimental data to an Arrhenius type of dependence $[N \propto \exp(-\Delta H_v/RT_{win})]$, with values of the correlation coefficient greater than 0.99, which suggests that the procedure is adequate. This type of dependence between MD flux and temperature has been used in other MD studies [3,8,28].

According to the second method presented in the Section 3, in Fig. 5 the reciprocal of the global MD coefficient is plotted as function of the inverse of the water circulation velocity, raised to the power n. The values of B were obtained from the experimental data presented in Fig. 2, that is, for water flowing in the shell side. The numerical value of the exponent n is chosen as that giving the best linear fit of the experimental data points. This procedure was applied, for each water temperature.

The obtained n values were found to vary between 0.57 and 0.60 and the correlation coefficients were, at least, 0.994.

As $(1/v_w)^n$ approaches to zero, which means that the water circulation velocity goes to infinity, the temperature at the membrane surface approaches the temperature at the bulk phase. In other words, the net and global MD coefficients become equal, $B' = B$ [2,12]. In this case, from the intercept of the graphs in Fig. 5, the net MD coefficients may be obtained, for each water

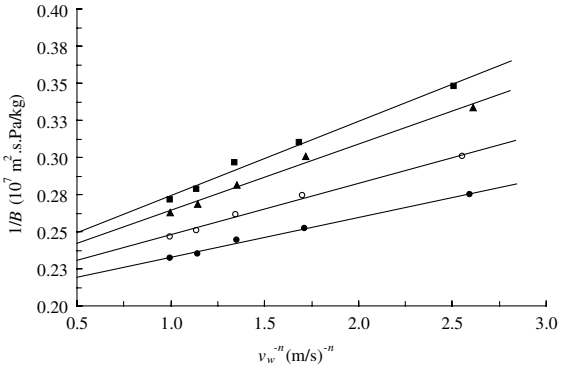

Fig. 5. Reciprocal of the global MD coefficient $(1/B)$ versus $(1/v_w^n)$, for different water temperatures: 40 °C (●); 50 °C (○); 60 °C (▲) and 65 °C (■). The solid lines represent the best lineal fits of the data.

temperature. The obtained B' values together with their standard errors are: (4.85 ± 0.05) $(10^{-7}$ kg/m^2 s Pa), (4.70 ± 0.06) $(10^{-7}$ kg/m^2 s Pa), (4.55 ± 0.09) $(10^{-7}$ kg/m^2 s Pa) and (4.46 ± 0.11) $(10^{-7}$ kg/m^2 s Pa), for water temperature of 40, 50, 60 and 65 °C, respectively. The net MD coefficient decreases slightly with temperature. This trend agrees with the Knudsen diffusion model discussed previously. It must be pointed out that the obtained values of B' are close to the theoretical ones calculated from Eq. (3) and assuming a tortuosity factor of 2 as it was suggested in [7,29]. To be more rigorous, the experimental values of B' were lower than the predicted ones to within 1% and 6%, over the temperature range investigated. This means that the procedure is adequate. Note that this procedure is difficult to use in the case of water flowing in the lumen side, because of changes in the nature of the flow regime.

According to Eq. (4), the values of the fluxes may be converted into the corresponding values of the heat transfer coefficient of the liquid feed boundary layer. It was observed that an increase in the water circulation velocity is accompanied by an increase in the MD flux and a corresponding increase in the heat transfer coefficient. This can be attributed to a reduction in the temperature polarisation effect [1–3]. As the heat transfer coefficient increases, the temperature at the membrane surface approaches to the bulk temperature and the vapour pressure driving force increases. Moreover, as observed for the MD flux, the heat transfer coefficient is greater when the liquid feed is circulated in the lumen side, and increases with the water temperature.

Finally the heat transfer coefficient was expressed as the dimensionless Nusselt number. The constants a, b and c appearing in Eq. (8) were determined as follows: First, a log–log plot of Nusselt number versus Reynolds number is made to estimate the dependence of the heat transfer on the Reynolds number, that is, on the water

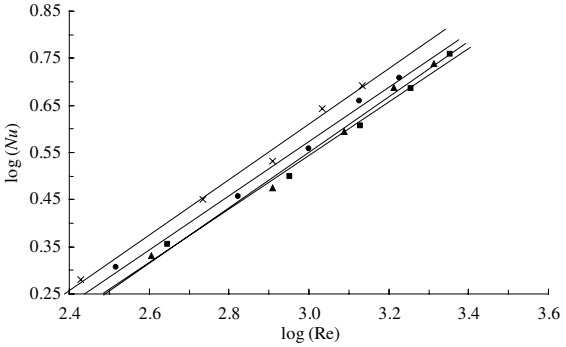

Fig. 6. log(Nu) versus log(Re) for constant water inlet temperature 40 °C (×), 50 °C (●), 60 °C (▲) and 65 °C (■). The solid lines are linear fits of the data in shell side.

circulation velocity. This permits to get an approximate value of the exponent b. This plot type is made for each water temperature so the influence of the Prandtl number will be small. In this case, a linear least square analysis of the experimental values ($\log Nu$) versus ($\log Re$) is applied at each set of constant water temperature. Then, by using the obtained value of b, all the experimental data are plotted as log (Nu/Re^b) versus log(Pr) to determine the value of c, power of the Prandtl number, and the value of a.

In the case of water flowing in shell side, Fig. 6 shows the plots of log(Nu) versus log(Re) for the temperatures 40 , 50, 60 and 65 °C. The obtained values of b together with their associated standard errors are presented in Table 1. It is worth mentioning that these values are almost the same as the exponent n values obtained from Eq. (7). As stated earlier, this is because Eq. (6) was obtained from the dependence of the Nusselt number, which is proportional to the heat transfer coefficient, on the Reynolds number, which is proportional to the circulation velocity, by means of Eq. (8). Again, this result confirms that the procedure used to determined the net MD coefficient, B', is adequate.

For each value of b ranging between 0.57 and 0.60, a plot of log(Nu/Re^b) versus log(Pr) was made. The estimated lineal fit parameters a and c and their associated standard errors are presented in Table 2. As an example, Fig. 7 shows a graph for the particular case when $b = 0.59$. The solid line is the least-squares fit of the experimental data points and the dashed lines represent

Table 1
b values from fits of Eq. (8) using a log–log plot of Nu versus Re

T_{win} (°C)	b	Correlation coefficient
40	$(59 \pm 3)\ 10^{-2}$	0.996
50	$(57 \pm 3)\ 10^{-2}$	0.997
60	$(59 \pm 3)\ 10^{-2}$	0.996
65	$(58 \pm 3)\ 10^{-2}$	0.997

Table 2
Values of c and a, from fits of Eq. (8) using a log–log plot of the factor (Nu/Re^b) versus Pr

b	c	a	Correlation coefficient
0.57	$(32 \pm 3)\ 10^{-2}$	$(486 \pm 8)\ 10^{-4}$	0.888
0.58	$(32 \pm 3)\ 10^{-2}$	$(448 \pm 7)\ 10^{-4}$	0.900
0.59	$(33 \pm 3)\ 10^{-2}$	$(413 \pm 6)\ 10^{-4}$	0.908
0.60	$(34 \pm 3)\ 10^{-2}$	$(380 \pm 6)\ 10^{-4}$	0.907

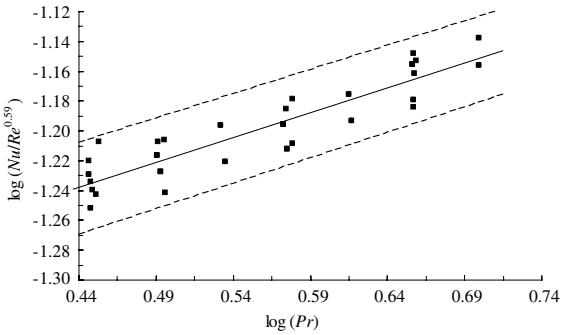

Fig. 7. log($Nu/Re^{0.59}$) versus log(Pr). The solid line is the linear fit of all data in shell side and the dashed lines represent 97.5% of confidence interval.

the 97.5% of confidence interval. As can be seen, all the experimental data points in shell side fall within this range. In general, the values of c, are very similar to the values given by most of the empirical correlations showed in the Section 3, for either internal or external flow (Eqs. (11), (12), (14)–(17)). As a summary, in Fig. 8, all experimental data in shell side are organised as a plot of the factor ($Nu/Pr^{0.33}$) versus Reynolds number. A final value of the exponent b is then determined as well as a value for the constant a, by fitting all the experimental data to a potential relation using the least squares analysis. Eq. (18) is the best fit of the experimental data

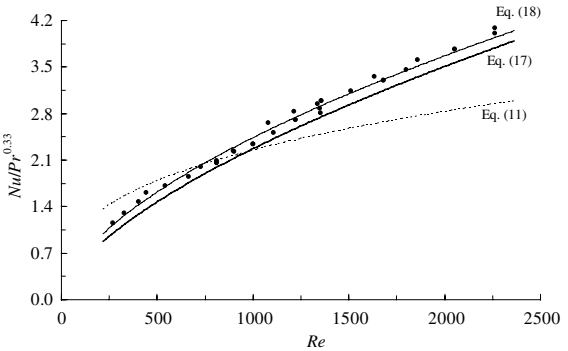

Fig. 8. Plot of the factor ($Nu/Pr^{0.33}$) versus the Reynolds number (Re) of all experimental data in shell side.

points for flow in shell side with a correlation coefficient of 0.996.

$$Nu = 0.042 \cdot Re^{0.59} \cdot Pr^{0.33} \tag{18}$$

This result is compared with other correlations published elsewhere. Firstly with the Groehn equation (Eq. (17)), and then, as an example of the correlations used for external flow in MD processes, it has been selected the Sieder and Tate equation in laminar flow (Eq. (11)).

As described in the Section 3, in this type of membrane modules both parallel and cross flow are taking place simultaneously. Our module has an equivalent yaw angle of 87° so we have more parallel flow than cross flow. As it is shown in Fig. 8, there is a slight increase of our data over those predicted by Eq. (17) over the entire range of the Reynolds number. The discrepancy between the experimental heat transfer coefficients and the corresponding values predicted by Eq. (17) is about 6.5%.

As an example, the equation of Sieder and Tate (Eq. (11)) is showed. This equation has been employed in Ref. [19] for external flow over capillaries to calculate heat transfer coefficients in MD processes. The experimental data agree closely with this equation for Reynolds number in the range $444 \leqslant Re \leqslant 1000$. However, for Reynolds numbers out of this range ($Re < 444$ and $Re > 1000$) the experimental data do not follow Eq. (11).

In the case of water circulating in lumen side, the experiments include both laminar and transitional flow. The procedure utilised in the case of flow in shell side is difficult to use in this case for all experimental data. This procedure is used separately for experimental data in laminar flow and the corresponding in transitional flow and the obtained value of the index c, was (0.30 ± 0.06) with a correlation coefficient of 0.983 and (0.32 ± 0.03) with a correlation coefficient of 0.943, for laminar and transitional flow regimes, respectively. As was observed in the case of water flow in shell side, the index c value is close to 0.33 (see Eqs. (11), (12), (14)–(17)). Finally, in Fig. 9, the factor $(Nu/Pr^{0.33})$ is plotted as function of the Reynolds number using all experimental data corresponding to water flow in lumen side.

Fig. 9 shows clearly a gradual transition between the laminar and turbulent limits presented by the solid lines (Eq. (11) at $Re \leqslant 2100$, Eq. (14) at $2100 < Re < 5000$ and the extrapolation of the Eq. (14) at low Reynolds number). In our opinion, the results for flow inside the capillaries agree worse with the empirical correlations for flow in laminar regime than in transitional regime.

In the laminar region, the experimental heat transfer coefficients are higher than the calculated ones using the proposed empirical correlations for laminar flow (Eqs. (9)–(13)), especially at Reynolds numbers close to 2100. To be more rigorous, a comparison between the experimental heat transfer coefficients and the values predicted from (Eqs. (9)–(13)) was made on the basis of the minimum weighed standard deviation, σ_w, defined as:

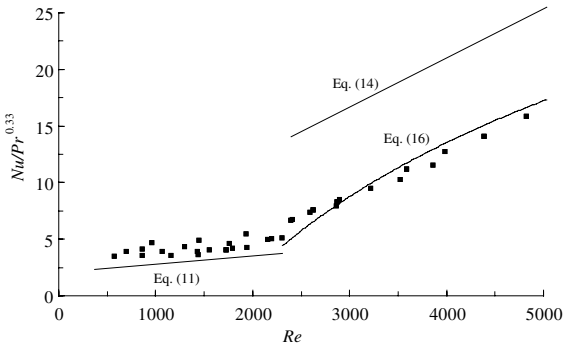

Fig. 9. Plot of the factor $(Nu/Pr^{0.33})$ versus the Reynolds number (Re) of all experimental data in lumen side.

$$\sigma_w = \left[\frac{1}{j-1} \sum_{i=1}^{j} \left(\frac{h_{(w,theo.)i}}{h_{(w,exp.)i}} - 1 \right)^2 \right]^{1/2} \tag{19}$$

where j is the number of experimental data points. The obtained values of σ_w were: 0.29, 0.22, 0.25, 0.34 and 0.34 applying Eqs. (9)–(13), respectively. Note that the minimum error was found when applying Eq. (10). Eq. (13), which is based on heat transfer experiments including free convection, was expected to augment the heat fluxes. However, in this case, according to the analysis performed in Refs. [14,30], the influence of the free convection is negligible as the calculated factor (Gr/Re^2) is below unity and the deviations between the experimental and the calculated heat transfer coefficients were maintained high. In general, the present experimental data do not fit well the traditional heat transfer correlations for laminar flow in lumen side. Consequently, when one applies the proposed correlations for internal laminar flow, a great error is introduced at the determination of the heat transfer coefficients, which will increase the MD modelling error. Also, at Reynolds numbers higher than 2100, neither the Dittus–Boelter correlation (Eq. (14)) nor the Sieder and Tate one (Eq. (15)) should be used. As shown in Fig. 9, the experimental heat transfer coefficients are lower than the calculated ones at high Reynolds numbers.

In the transition region, the heat transfer grows with the Reynolds number, apparently approaching the turbulent heat transfer limit in Eq. (14) at high Reynolds numbers. Hausen's correlation for flow in transitional regime (Eq. (16)) provides a reasonable description of the data. The discrepancy between the experimental heat transfer coefficient and the transitional heat transfer result in Eq. (16) is only about 10% for Reynolds numbers higher than 2000. It is worth noticing that in our case the critical Reynolds number is not so clearly defined, it may be between 2000 and 2400.

Generally speaking, our data do not fit all the traditional heat transfer correlations for neither external flow in shell side or for internal flow in lumen side, especially in the regime corresponding to low Reynolds number. The difference observed between the theoretical and the experimental Nusselt numbers can be due to several causes. The most important cause is that the conditions and processes of experimental operation differ appreciably, and the boundary conditions of constant wall temperature or constant heat flux are not strictly valid because of the influence of the mass transfer through the membrane. Additionally, the membrane may deform under excess external pressure conditions (high pressure on the shell side). This leads to a change of tube side flow area and will lead to inaccuracies in the determination of the tube side Reynolds and Nusselt numbers. Besides, the presence of the capillary membrane type may act as a turbulence promoter, which will reduce the boundary layer thickness adjacent to the membrane surface. In addition, more turbulence may occur due to the roughness of the microporous MD membranes. On the other hand, there may be irregular distribution of flow through each one of the capillaries as the membrane material is soft. This fact will influence the uniformity of the MD flux within the membrane module. In this sense, the characteristic constants of the heat transfer empirical correlations must be re-evaluated for heat transfer calculations in MD systems.

5. Conclusions

An experimental study of VMD processes, in a shell-and-tube capillary membrane module was presented. The effect of the water circulation velocity and temperature on the MD flux has been discussed. A method to estimate the feed boundary layer heat transfer coefficients in both lumen and shell sides of the capillary membrane module has been presented. A critical review of most frequently used heat transfer empirical correlations in MD is presented. The results show that:

(1) An increase in the water circulation velocity is accompanied by an increase in the MD flux and a corresponding increase in the heat transfer coefficient in the liquid feed boundary layer. This can be attributed to a reduction in the temperature polarisation effect.
(2) The MD flux is strongly dependent on the water temperature, following an Arrhenius type of dependence and the heat transfer coefficient increases with this parameter.
(3) The MD flux and the heat transfer coefficient are greater when the liquid feed is circulated in the lumen side than in the shell side.
(4) The applicability of the heat empirical correlations most frequently used in MD processes has been checked.

For flow in shell side, the experimental results agree with Groehn's equation (Eq. (17)) in about 93.5%. On the contrary, do not agree with the Eqs. (9)–(13) performed for internal laminar flow.

For flow in lumen side, the empirical correlations in laminar regime (Eqs. (9)–(13)) and turbulent regime (Eqs. (14) and (15)) agree worse with the experimental data than in transitional regime (Eq. (16)).

Special care must be taken into account when one uses the empirical correlations obtained for "pure" heat exchangers. The characteristic constants must be re-evaluated for heat transfer calculations in MD processes.

Acknowledgements

Economical support from the CICYT is acknowledged.

References

[1] K.W. Lawson, D.R. Lloyd, Membrane distillation, J. Membrane Sci. 124 (1997) 1–25.
[2] J.I. Mengual, L. Peña, Membrane distillation, Colloid Surf. Sci. 1 (1997) 17–29.
[3] R.W.A. Schofield, A.G. Fane, C.J.D. Fell, Heat and mass transfer in membrane distillation, J. Membrane Sci. 33 (1987) 299–313.
[4] M. Khayet, M.P. Godino, J.I. Mengual, Theory and experiments on sweeping gas membrane distillation, J. Membrane Sci. 165 (2) (2000) 261–272.
[5] M. Khayet, M.P. Godino, J.I. Mengual, Nature of flow on sweeping gas membrane distillation, J. Membrane Sci. 170 (2) (2000) 243–255.
[6] E.A. Mason, A.P. Malinauskas, Gas Transport in Porous Media: The Dusty-Gas Model, Elsevier, Amsterdam, 1983, pp. 30–42.
[7] S. Bandini, A. Saavedra, G.C. Sarti, Vacuum membrane distillation: experiments and modeling, AIChE J. 43 (1997) 398–408.
[8] J.M. Ortiz de Zárate, F. García-López, J.I. Mengual, Temperature polarisation in non-isothermal mass transport through membranes, J. Chem. Soc.- Faraday Trans. 86 (16) (1990) 2891–2896.
[9] L. Martínez-Díez, M.I. Vázquez-González, Temperature polarisation in mass transport through hydrophobic porous membranes, AIChE J. 42 (1996) 1844–1852.
[10] S. Bandini, C. Gostoli, G.C. Sarti, Separation efficiency in vacuum membrane distillation, J. Membrane Sci. 73 (1992) 217–229.
[11] K.W. Lawson, D.R. Lloyd, Membrane distillation: I module design and performance evaluation using vacuum

membrane distillation, J. Membrane Sci. 120 (1996) 111–121.
[12] M. Khayet, M.P. Godino, J.I. Mengual, Modeling transport mechanism through a porous partition, J. Non-Equilibrium Thermodyn. 26 (2001) 1–14.
[13] A. Velázquez, J.I. Mengual, Temperature polarisation coefficients in membrane distillation, Indust. Eng. Chem. Res. 34 (2) (1995) 585–590.
[14] F. Kreith, M.S. Bohn, Principle of Heat Transfer, fifth ed., PWS Publish. Comp., Boston, 1997, pp. 445–497.
[15] J.P. Holman, Heat Transfer, seventh ed., McGraw-Hill Book Company, Singapore, 1989, pp. 271–321.
[16] G.C. Sarti, C. Gostoli, S. Bandini, Extraction of organic components from aqueous streams by vacuum membrane distillation, J. Membrane Sci. 80 (1993) 21–33.
[17] M. Gryta, M. Tomaszewska, Heat transport in the membrane distillation process, J. Membrane Sci. 144 (1998) 211–222.
[18] M. Tomaszewska, M. Gryta, A.W. Morawski, Mass transfer of HCL and H_2O across the hydrophobic membrane during membrane distillation, J. Membrane Sci. 166 (2000) 149–157.
[19] F.A. Banat, A. Abu Al-Rub, R. Jumah, M. Al-Shamag, Modeling of desalination using tubular direct contact membrane distillation modules, Separat. Sci. Technol. 34 (11) (1999) 2191–2206.
[20] L. Martínez-Díez, M.I. Vázquez-González, Temperature and concentration polarisation in membrane distillation of aqueous salt solutions, J. Membrane Sci. 156 (1999) 265–273.
[21] S. Kimura, S.I. Nakao, S.I. Shimatani, Transport phenomena in membrane distillation, J. Membrane Sci. 33 (1987) 285–298.
[22] V. Ugrozov, I.B. Elkina, A selectivity model for membrane distillation of solutions of non-volatile salts, Russ. J. Phys. Chem. 70 (1996) 1670–1674.
[23] L. Martínez-Díez, M.I. Vázquez-González, Effect of polarisation on mass transport through hydrophobic porous membranes, Indust. Eng. Res. 37 (1998) 4128–4135.
[24] Y. Fujii, S.K. Hidestsugu Iwatani, M. Aoyama, Selectivity and characteristics of direct contact membrane distillation type experiment: I. permeability and selectivity through dried hydrophobic fine porous membranes, J. Membrane Sci. 72 (1992) 53–72.
[25] H. Gröber, S. Erk, Transmisión de Calor, 1st Spanish ed., Selecciones Científicas, Madrid, 1967, pp. 256–288.
[26] S. Bandini, G.C. Sarti, Heat and mass transport resistances in vacuum membrane distillation per drop, AIChE J. 45 (1999) 1422–1433.
[27] M.P. Godino, L. Peña, J.I. Mengual, Membrane distillation: theory and experiments, J. Membrane Sci. 121 (1996) 83–93.
[28] E. Drioli, Y. Wu, Membrane distillation: an experimental study, Desalination 53 (1985) 339–346.
[29] C. Gostoli, Thermal effects in osmotic distillation, J. Membrane Sci. 163 (1999) 75–91.
[30] E.C. Guyer, D.L. Brownell, Handbook of Applied Thermal Design, McGraw-Hill Book Company, New York, 1989, pp. (1) 31–47.